ROYAL SOCIETY OF CHEMISTRY

www.rsc.org/dalton

Journal Name

Dalton Transactions

ARTICLE TYPE

Influence of the central diamagnetic cyanidometal on the distant magnetic interaction in cyanide-bridged Fe(III)-M(II)-Fe(III) complexes

Yong Wang,[a] Chensheng Lin,[a] Xiao Ma,[a] Zhenzhen Xue,[a] Xiaoquan Zhu,[a] Wenhai Cao,[a] Shengmin Hu,[a] Tianlu Sheng*[a] and Xintao Wu[a]

To investigate how the central diamagnetic cyanidometal influences the distant magnetic interaction of cyanide-bridged Fe(III)-M(II)-Fe(III) complexes, *cis*-[Cp(dppe)Fe^{II}(NC)M^{II}(L)$_2$(CN)Fe^{II}(dppe) Cp][PF_6]$_2$ (M = Os, L = bpy **1**; M = Os, L = phen **2**; M = Fe, L = bpy **3**; M = Fe, L = phen **4**), and their one-electron
10 oxidation products **5-7** and two-electron oxidation products **8-11** were synthesized and fully characterized. The cyclic voltammetry of complexes **1-4** suggests that both NC-Os^{II}(L)$_2$-CN and NC-Fe^{II}(L)$_2$-CN have electronic communication ability. The electronic absorption spectroscopy suggests the presence of the central M^{II} to the terminal Fe^{III} and the terminal Fe^{II} to the terminal Fe^{III} metal to metal charge transfers (MMCTs) in **5-7** and the central M^{II} to the terminal Fe^{III} MMCTs in **8-11**. Moreover, for
15 the two-electron oxidation products the MMCT energy increases with the central metal of the order Fe < Os < Ru. The two-electron oxidation complexes **8** and **9** exhibit a strong antiferromagnetic coupling ($J \approx$ -26 cm^{-1}) between the two distant Fe^{III} ions although separated by the diamagnetic cyanidometal NC-Os^{II}(L)$_2$-CN bridge. To the best of our knowledge, this is the strongest magnetic coupling between the distant paramagnetic metal ions across a diamagnetic cyanidometal bridge reported by far. For the two-
20 electron oxidation complexes **10** and **11** with the diamagnetic NC-Fe^{II}(L)$_2$-CN bridge, however, the distant two Fe^{III} ions posses only very weak antiferromagnetic coupling (J = -0.15 and -0.19 cm^{-1}). Combined with our previous reported results, it could be found that the magnetic coupling strength between the distant Fe^{III} ions increases with the diamagnetic cyanidometal bridge in the order of Fe < Ru < Os.

Introduction

25 In the past decades, cyanide-bridged complexes with fascinating magnetic properties have received considerable attention due to their potential applications as photomagnetic materials[1], high T_c magnets[2], single-molecule magnets[3], single-chain magnets[4], and spin crossover
30 materials[5]. However, taking a diamagnetic cyanidometal as a magnetic-communication bridge is still paid much less attention by magnetochemists, although the work aimed at distant metal-metal interactions in cyanide bridged trinuclear complexes was performed by us[6-9] and other groups.[10] The reasons may be as follows: 1) The
35 magnetic interaction between two paramagnetic metal centres decreases rapidly and even disappears when the distance between the paramagnetic metal centres increases; 2) The validity of the intramolecular magnetic interaction of such complexes is often questionable, since it is easy to erroneously attribute the effects of
40 intermolecular magnetic exchange to weak intramolecular superexchange.[11] Therefore, the design and synthesis of such polynuclear complexes with a strong distant magnetic coupling is still a challenge. To date, only a few examples of such complexes with weak magnetic interaction have been reported.[12] Recently, our
45 research interests have been focused on investigating the distant

magnetic coupling across a diamagnetic cyanidometal bridge.[6-9] We have reported that the distant Fe^{III} centres exhibit strong magnetic coupling (J = -13.6 cm^{-1}) even though the two distant Fe^{III} centres are separated by the diamagnetic cyanidometal NC-Ru^{II}-CN bridge.[7] The
50 theoretical investigation has shown that the spin delocalization mechanism should be responsible for the strong magnetic coupling.[13] Thus, we are interested to investigate how the magnetic coupling between the distant Fe^{III} ions is influenced by the central diamagnetic cyanidometal bridge. To understand this, M^{II}(L)$_2$(CN)$_2$ (M = Os, Fe;
55 L = bpy, phen, bpy = 2, 2'- bipyridine, phen = 1, 10 - phenanthroline) were selected as the diamagnetic bridge due to their different radial extension of the *d* orbitals and their different degree of electron density delocalization over the cyanide groups with respect to Ru^{II}(L)$_2$(CN)$_2$.[14] Herein, we report the syntheses and
60 characterizations of [Cp(dppe)Fe^{II}(NC)M^{II}(L)$_2$(CN)Fe^{III}(dppe)Cp] [PF_6]$_2$ (M = Os, L = bpy **1**; M = Os, L = phen **2**; M = Fe, L = bpy **3**; M = Fe, L = phen **4**) (dppe = bis(diphenylphosphino) ethane, Cp = cyclopentadienide anion), their one-electron oxidation products [Cp(dppe)Fe^{II}(NC)M^{II}(L)$_2$(CN)Fe^{III}(dppe)Cp][PF_6]$_3$ (M = Os, L = bpy
65 **5**; M = Os, L = phen **6**; M = Fe, L = phen **7**) and their two-electron oxidation products [Cp(dppe)Fe^{III}(NC)M^{II}(L)$_2$(CN)-Fe^{III}(dppe)Cp][PF_6]$_4$ (M = Os, L = bpy **8**; M = Os, L = phen **9**; M = Fe, L = bpy **10**; M = Fe, L = phen **11**). The MMCT properties of all

the oxidized products **5-11** are reported. The magnetic properties of the two-electron oxidation products **8-11** were measured and are discussed, and the results show that the magnetic coupling strength between the distant Fe^{III} centres increases with the diamagnetic
5 cyanidometal bridge in the order of Fe^{II} < Ru^{II} < Os^{II}.

Results and Discussion

Synthesis and characterization

Reaction of *cis*-Os^{II}(L)$_2$(CN)$_2$ (L = bpy, phen) with Cp(dppe)Fe^{II}(NCCH$_3$)Br in the presence of NH$_4$PF$_6$ gave rise to
10 the expected tri-nuclear complexes **1** and **2**, respectively. Based on the electrochemical oxidation potentials of **1** and **2** (vide infra), Cp$_2$Fe^{III}(PF$_6$) and AgPF$_6$ were chosen as oxidants for the preparation of the oxidation species. Treatment of **1** and **2** with one equiv of Cp$_2$Fe^{III}(PF$_6$) resulted in the solution colour
15 changing from red to brown and gave one-electron oxidation products **5** and **6**. The two-electron oxidation products **8** and **9** were prepared in a similar way by reaction of **5** and **6** with 1 equiv of AgPF$_6$. The syntheses of **3** and **10** were performed as previously reported by Vahrenkamp[15], and their structures had
20 not been obtained. Similar to the previous report[15], however, the one-electron oxidation product of **3** could not be obtained. Complexes **4**, **7** and **11** were obtained in a similar way as complexes **1**, **5** and **8**. All complexes **1-11** were characterized by IR, electronic absorption spectra, elemental analysis, MS and
25 cyclic voltammetry. Moreover, the crystals of **1-4** and **6-10** suitable for the single-crystal X-ray diffraction analysis were obtained by slow diffusion of diethylether into their dichloromethane or acetonitrile solution.

Crystal structures

30 Experimental crystallographic data for complexes **1-3** are given in Table S1 in Supporting Information, and **4** and **6-10** are given in Table 1. Selected bond lengths and angles for **1-3** are given in Table S2, and **4** and **6-10** are given in Table 2. The molecular structures of **1-4** and **6-10** are shown in Figures S1-S9,
35 respectively. The crystals crystallize in the monoclinic space group *P*2$_1$/n for **1**, orthorhombic space group *Pbca* for **2** and **4**, and monoclinic space group *P*2$_1$/c for **3** and **6-10**, respectively. The backbone of all the trinulcear complexes adopts a V-shaped configuration. The structures are composed of two terminal
40 CpFe(dppe) fragments bridged by a central low spin diamagnetic M(L)$_2$(CN)$_2$ (M = Fe and Os) bridge. The central M atom defines a distorted octahedral coordination environment, and is linked by four nitrogen atoms from the bpy or phen ligands and the remaining two sites are coordinated by two carbon atoms from
45 the cyanide groups with a *cis* configuration.

As oxidation proceeds, the bond lengths of Fe-N decrease from **1** (av. 1.906 Å) to **8** (av. 1.881 Å) and those of Fe-P increase from **1** (av. 2.195 Å) to **8** (av. 2.256 Å), indicating the character of +2 and +3 oxidation state of the two Fe centres in **1** and **8**,
50 respectively. Similarly, an obvious change in the bond lengths of Fe-P can also be found for **2**, **6** and **9**. For **2**, the bond length of Fe1-P (av. 2.198 Å) is close to that of Fe2-P (av. 2.192 Å) and comparable to that of Fe-P in **1**. As one-electron oxidation proceeds, the different oxidation states of Fe1 (+2) and Fe2 (+3)
55 in the mixed valence complex **6** are also supported by the fact that the bond length of Fe1-P (av. 2.203 Å) is shorter than that of

Fe2-P (av 2.253 Å) due to the less back-binding from Fe2 to the phosphorus ligands. As further oxidation proceeds, both the comparable bond lengths of Fe1-P (av. 2.268 Å) and Fe2-P (av.
60 2.252 Å) in **9** are close to that of Fe2-P (av 2.253 Å) in **6**, indicating the character of +3 oxidation state of the two Fe centres in **9**.

The facts that the bond lengths of Fe-N decrease from **3** (av. 1.926 Å) to **10** (av. 1.899 Å) and the bond lengths of Fe-P increase from **3**
65 (av. 2.200 Å) to **10** (av. 2.262 Å), indicate the oxidation states of the two Fe centres are +2 in **3** to +3 in **10**, respectively. The Fe-P bond lengths (Fe1-P (av. 2.197Å) and Fe2-P (av. 2.197 Å)) and Fe-N bond lengths (Fe1-N (1.920(3) Å) and Fe2-N (1.921(3) Å) in **4** are close to those in **1-3**, suggesting the character of +2
70 oxidation state of the two Fe centres in **4**. The different oxidation state of Fe1 (+3) and Fe2 (+2) in **7** can also be found from their Fe-P bond lengths (Fe1-P, av 2.263 Å; Fe2-P, av 2.202 Å) and Fe-N bond lengths (Fe1-N, 1.888(4) Å; Fe2-N, 1.910(4) Å).

The bond distances of M^{II}-C (1.953(13) and 1.976(14) Å) in **1** and
75 (1.950(4) and 1.953(4) Å) in **8** are longer than those in **3** (1.932(7) and 1.921(7) Å) and **10** (1.879(3) and 1.884(3) Å) due to the larger radii of Os^{II} than Fe^{II}. The similar phenomenon can also be found in the phen-based complexes that the bond distance of M^{II}-C in **2** (1.997(13) and 2.003(13) Å) and **6** (1.966(10) and
80 1.912(11) Å) are longer than those in **4** (1.904(4) and 1.916(4) Å) and **7** (1.865(5) and 1.908(5) Å).

The bond angles of C-M-C increase in the order of 94.2(5)° (**1**) < 95.8(2)°(**8**), 92.1(4)° (**2**) < 93.4(4)° (**6**) < 94.5(2)° (**9**), 91.9(3)° (**3**) < 95.7(3)°(**10**) and 91.8(2)° (**4**) < 94.0(2)° (**7**). This changes can
85 be explained by the increase of electrostatic repulsion force between the intramolecular positively charged iron centres from **1-4** to **6-10**, respectively. For **1-10**, The shortest intramolecular Fe···M (M is the central metal Os or Fe) distances are 4.9 - 5.1 Å, the nearest bond-through Fe···Fe distances across the diamagnetic
90 cyanidometal NC-M^{II}-CN bridge are 9.9 - 10.2 Å, whereas the intramolecuar space-through Fe···Fe separations are 7.44-7.95 Å. It should be noted that the shortest intermolecular distances of Fe···Fe are 9.485, 7.155 and 9.630 Å for **8**, **9** and **10**, respectively.

Electrochemistry

95 Cyclic voltammetry studies were carried out on **1-4** to determine their redox properties, as well as to establish whether the oxidation products were stable and potentially isolable. The cyclic voltammograms of complexes **1-4** in the acetonitrile solution are shown in Figure 1. The cyclic voltammograms show
100 two reversible redox waves at +0.22 and +0.39 V for **1**, +0.22 and +0.38 V for **2**, +0.29 and +0.41 V for **3**, and +0.28 and +0.40 V for **4**, respectively. These two waves are assigned to Fe^{II}–M^{II}–Fe^{II}/Fe^{II}–M^{II}–Fe^{III} and Fe^{II}–M^{II}–Fe^{III}/Fe^{III}–M^{II}–Fe^{III} processes. This suggests that the one-electron and two-electron oxidation
105 products may be stable and potentially isolable for complexes **1-4**. More importantly, the potential splitting of the complexes suggest that the NC-Os^{II}-CN and NC-Fe^{II}-CN bridges can communicate electron between the two distant iron centres.

The potential separation of the Fe^{II} ions in the Os(II)-based
110 complexes (ΔE =170 mV (**1**) and 160 mV(**2**)) are larger than that in the Ru(II)-based complexes[6-8] (ΔE = 110 mV) and Fe(II)-based complexes (**3** and **4**, ΔE = 120 mV). It has been known that the comproportionation constant (K_c) is associated with the thermodynamic stability of mixed valence complexes. According

to $K_c = 10^{\Delta E/59mV}$,[16] where ΔE corresponds to the difference measured by cyclic voltammetry of the half-wave potentials for the first and second oxidations, it can be obtained that K_c for **5**, **6** and **7** is 761, 515 and 108, respectively.

IR spectroscopy

To monitor the structural changes during the consecutive oxidation of complexes **1-11**, the IR spectra in the solid state samples (KBr pellets) are collected. The cyanide stretching vibration (ν_{CN}) is extremely sensitive to the coordination environment to metal centres. The IR data for the CN stretching frequencies for complexes **1-11** are listed in Table 3, and the infrared spectra of **1**, **5** and **8** are shown in Figure 2, **2**, **6** and **9** in Figure 3. Complex **1** exhibits a broad ν_{CN} band (2074 cm^{-1}) with a shoulder peak (2091 cm^{-1}). Obviously, the ν_{CN} band position moves to the higher frequency with respect to those in its precursor *cis*-Os(bpy)$_2$(CN)$_2$ (2057, 2040 cm^{-1}).[17, 18] Such a frequency increase is mainly attributed to both kinematical coupling occurring when a second metal is attached to the CN unit and the fact that the cyanide N donated electron density from an anti-bonding molecular orbital to the Fe^{II} centre, thereby increasing the CN force constant.[19] As one-electron oxidation proceeds, the mixed-valence complex **5** exhibits two evidently separated ν_{CN} bands (2074 cm^{-1} and 1992 cm^{-1}). The two N atoms of CN are respectively attached to the Fe atoms with different positive charges in **5**, hence, it can be concluded that the low frequency band (1992 cm^{-1}) should be assigned to the CN group attached to the Fe^{III} atom due to the increase of the back-bonding effect from the central Os^{II} into the CN bond by the withdrawal of electron from the cyanide to Fe^{III} resulting in the lower ν_{CN} energy.[19] The band of 2074 cm^{-1} should be assigned to the CN group attached to the Fe^{II} atom which environment is similar to that of complex **1**. For the two-electron oxidation product **8** two ν_{CN} bands (2039 cm^{-1} and 1987 cm^{-1}) appear, resulting from the combination of symmetric and asymmetric stretching frequencies in a *cis*-configuration. Both the bands are significantly red-shifted relevant to those in **1**, this can be explained by the enhancement of the π back-bonding from the carbon-bound metal (Os^{II}) into the CN bond due to the cyanide is coordinated to the electron-attracting Fe^{III} ions, leading to a weakening of the C≡N bond and hence resulting in a shift to lower frequency for CN.[19] Similarly, the ν_{CN} band changes from **2** (2072 cm^{-1}) to **6** (2072 cm^{-1}, 1993 cm^{-1}) to **9** (2042 cm^{-1},1993 cm^{-1}), from **3** (2094 cm^{-1}) to **10** (2035 cm^{-1}),[15] and from **4** (2094cm^{-1}) to **7** (2094 cm^{-1}, 2033 cm^{-1}) to **11** (2032 cm^{-1}).

Moreover, it is worth noting from Table 3 that the cyanide stretching (ν_{CN}) of the mononuclear complexes M(L)$_2$(CN)$_2$[17, 18, 20] decreases in the order Fe > Ru > Os, suggesting the degree of electron density delocalization over the cyanide groups from M^{II} increases in the order of Fe < Ru < Os. The increasing order of the electron density delocalization is also reflected in the ν_{CN} changes of the trinuclear complexes **1-11**. For example, ν_{CN} of the unoxidized complexes **1**, **3** and the analogues *cis*-Ru(bpy)$_2$(CN)$_2$-bridged complex[9c] decreases with the order of Fe (2094 cm^{-1}) > Ru (2086 cm^{-1}) > Os (2074 cm^{-1}). Also, for the two-electron oxidation products of **8**, **10** and the analogues *cis*-Ru(bpy)$_2$(CN)$_2$-bridged complex[9c] the ν_{CN} band decreases in the order of Fe (2035 cm^{-1})> Ru (2021 cm^{-1})[7]> Os(1987 cm^{-1}). The

similar phenomena have been in detail studied by other chemists.[21]

UV-vis-NIR spectroscopy

In order to investigate the electronic properties of complexes **1-11** with different oxidation states, their electronic absorption spectra were measured in the CH$_3$CN solution at room temperature. The electronic spectra of **1**, **5** and **8** are shown in Figure 4, **2**, **6** and **9** in Figure 5, **3** and **10** in Figure S10, and **4**, **7** and **11** in Figure S11. And the related data are summarized in Table 3. Obviously, the NIR bands related to MMCT should be focused. For those UV-vis absorptions below 700 nm, only complex **1** is discussed.

The formation of the cyanide-bridged complex **1** is accompanied by the appearance of the bands at λ_{max} of 387, 500 and 695 nm. The former two bands can be assigned to d→π* MLCT (metal to ligand charge transfer).[8] The band at λ_{max} of 695 nm may be assigned to ^{3}MLCT transition, being red-shifted by 45 nm with respect to 650 nm of *cis*-Os^{II}(bpy)$_2$(CN)$_2$[17]. As one-electron-oxidation proceeds, a new NIR band at λ_{max} of 910 nm appears in **5**, which can be assigned to the mixture of the central Os^{II}→ terminal Fe^{III} and the distant terminal Fe^{II}→terminal Fe^{III} metal-to-metal charge transfers (MMCTs) based on the TDDFT (time-dependent density functional theory) calculations (see Supporting Information). It can also be found that **2** does not exhibit any absorption band in the NIR region, but its one-electron oxidation product **6** displays a relatively intense NIR band at λ_{max} of 912 nm, which could also be attributed to the mixture of the central Os^{II}→ terminal Fe^{III} and the distant terminal Fe^{II}→ terminal Fe^{III} MMCTs. Similarly, the band at λ_{max} of 1217 nm in **7** should also be assigned to the mixture of the central Fe^{II}→ terminal Fe^{III} and the distant terminal Fe^{II}→terminal Fe^{III} MMCTs. Upon two-electron oxidation, the 910 nm band in **5** diminishes, and another intense band at λ_{max} of 896 nm appears in the two-electron-oxidation product **8**, which is assigned to the central Os^{II}→ terminal Fe^{III} MMCT. For the other two-electron-oxidation products **9-11**, their NIR bands at λ_{max} of 886, 1210 and 1172 nm can be attributed to the central Os^{II}→terminal Fe^{III} or the central Fe^{II}→terminal Fe^{III} MMCT, respectively. The shoulder bands near 1200 nm in Fig. 11 and 12 of should be resulted from spin-orbit coupling of complexes **5**, **6**, **8** and **9**.[22] By comparison of **8-11** with the analogous Ru^{II}(bpy)$_2$(CN)$_2$ (722 nm) and Ru^{II}(phen)$_2$(CN)$_2$ (717 nm) bridged complexes,[8] it can be found that the central M^{II} to terminal Fe^{III} MMCT energy increases with the central metal in the order Fe < Os < Ru. It is interesting that the order of the MMCT energy change is similar to that of the metal to bipyridine MLCT energy change found in the mononuclear M^{II}(bpy)$_3$(PF$_6$)$_2$ (M = Fe, Ru, Os) complexes.[23]

Based on the above MMCT band shape of mixed valence complexes **5-7**, **10** and **11**, all the mixed valence complexes should belong to Class II mixed valence complexes, according to the classification of Robin and Day.[24]

Magnetic properties

To investigate the magnetic exchange coupling between paramagnetic Fe^{III} ions across the diamagnetic cyanidometal NC-M^{II}-CN (M = Os, Fe) bridge, the temperature-dependent magnetic susceptibility measurements of **8-11** were performed at 1000 Oe in the temperature range of 2-300 K. The plots of $\chi_M T$

vs. T and χ_M vs. T of polycrystalline samples **8-11** were given in Figures 6-9, respectively, where χ_M is the molar magnetic susceptibility and T is the temperature in Kelvin. As shown in Figures 6 and 7, the $\chi_M T$ at 300 K of 0.746 cm^3 K mol^{-1} for **8** and 0.752 cm^3 K mol^{-1} for **9** are in good agreement with the expected value of 0.750 cm^3 K mol^{-1} for two uncoupled low-spin (LS) Fe^{III} and one diamagnetic LS Os^{II} ions ($S_{Fe(III)}$ = 1/2, $S_{Os(II)}$ = 0) on the basis of g = 2.0. The $\chi_M T$ values decrease slowly with decreasing temperature to 0.666 cm^3 K mol^{-1} at 120 K for **8** and 0.677 cm^3 K mol^{-1} at 112 K for **9**, and then sharply decrease to 0.105 cm^3 K mol^{-1} for **8** and 0.097 cm^3 K mol^{-1} for **9** at 2 K. The magnetic susceptibilities in 60-300 K range obey the Curie-Weiss law with negative Weiss constants of θ = -42.7 K for **8** and θ = -43.1 K for **9**. It indicates the presence of anti-ferromagnetic coupling in **8** and **9** based on the shape of $\chi_M T$ vs. T curves and the negative Weiss constants, which may attributed to the distant magnetic coupling between the Fe(III) ions across the diamagnetic cyanidometal NC–Os^{II}–CN bridge. Since the nearest intermolecular Fe^{III}···Fe^{III} distances are respectively 9.5 and 7.2 Å for **8** and **9**, the intermolecular magnetic interaction can be neglected. One may have concerned that the magnetic coupling of complexes **8** and **9** are resulted from the spin-orbit coupling of low-spin Fe^{III} ions. To investigate this, the temperature-dependence magnetic susceptibility measurement for the one-electron oxidation product **5**, in which the coordination environment of the only one paramagnetic low-spin Fe^{III} ion is very similar to those in **8** and **9**, was performed on the polycrystalline sample in the temperature of 2-300 K at an applied magnetic field of 1000 Oe. The $\chi_M T$ vs T plot is depicted in Figure S18. The $\chi_M T$ value of **5** is 0.341 cm^3 K mol^{-1}, which is close to the expected theoretical values of 0.375 cm^3 K mol^{-1} for one uncoupled LS Fe^{III} ($S_{Fe(III)}$ = 1/2), one diamagnetic LS Fe^{II} ($S_{Fe(II)}$ = 0) and one diamagnetic LS Os^{II} ions ($S_{Os(II)}$ = 0) assuming g = 2.0. Upon lowering the temperature, the $\chi_M T$ value remains constant until 30 K, then smoothly decreases to 0.300 cm^3 K mol^{-1} at 2 K. As expected, complex **5** is paramagnetic with an S = 1/2 spin ground-state. This suggests that the spin-orbit coupling of the low-spin Fe^{III} ion is very small and can be neglected in the system. Thus, it can conclude that the magnetic coupling of complexes **8** or **9** should be resulted from the intramolecular interaction between distant low-spin Fe^{III} ions. The mechanism has been studied and reported in our previous paper.[7] That is, the spin-delocalization mechanism[25] should be responsible for the strong magnetic interaction between the two distant paramagnetic Fe(III) centres across the diamagnetic NC-Os^{II}-CN bridge.

As shown in Figures 8 and 9, the $\chi_M T$ at 300 K is 0.741 cm^3 K mol^{-1} for **10** and 0.735 cm^3 K mol^{-1} for **11**. The values are close to the theoretical value of 0.750 cm^3 K mol^{-1} for two uncoupled low-spin (LS) Fe^{III} and one diamagnetic LS Fe^{II} ions ($S_{Fe(III)}$ = 1/2, $S_{Fe(II)}$ = 0) on the basis of g = 2.0. On lowering the temperature, the $\chi_M T$ values of complexes **10** and **11** keep almost a constant until 8 K, finally decreases to 0.701 cm^3 K mol^{-1} for **8** and 0.695 cm^3 K mol^{-1} for **11** at 2 K. The decrease of $\chi_M T$ at low temperature might be attributed to the zero-field splitting (ZFS) effect of Fe^{III} ions. The magnetic susceptibilities of **10** and **11** obey the Curie-Weiss law and could be fitted based on Curie-Weiss law, affording θ = -0.15 K for **8** and θ = -0.20 K for **11**.

From these observation, it indicates that the magnetic behaviors of **10** and **11** are very weak antiferromagnetic and even can be regarded as almost paramagnetic.

In order to evaluate the magnetic coupling (J) between Fe^{III} ions for **8** and **9**, the magnetic susceptibilities data are fitted with the Hamiltonian **H** = -2J **S**$_1$·**S**$_2$, and the following modified Bleaney-Bowers equation[26] were used: $\chi_M = 2Ng^2\beta^2/kT[3 + \exp(-2J/kT)]$ $(1-\rho)/+2Ng^2\beta^2\rho/3kT \times S(S+1)$, where N, g, k, ρ and β are the Avogadro number, the g-factor, the Boltzmann constant, molar fraction of noncoupled species and the Bohr magneton, respectively. Least-squares fitting of data of **8** and **9** in 60-300 K range leads to J = -25.8 cm^{-1}, g = 2.07, ρ = 1.12% and R = $(\Sigma(\chi_{calcd} T - \chi_{obsd} T)^2)/\Sigma(\chi_{obsd} T)^2$ = 2.0×10^{-5} for **8** and J = -26.1 cm^{-1}, g = 2.09, ρ = 3.19% and R = 8.0×10^{-5} for **9**. The fitting g-values are consistent with the values from the EPR spectroscopy (g = 2.01 for **8** in Figure S20 and g =2.05 for **9** in Figure S22). For the purpose of comparison, the magnetic susceptibilities of **10** and **11** were also fitted in the same way as **8** and **9**. The simulation results are J = -0.15 cm^{-1}, g = 1.98, ρ = 1.78% and R = 3.7×10^{-8} for **10** and J = -0.19 cm^{-1}, g = 1.98, ρ = 1.44% and R = 1.0×10^{-7} for **11**. The fitting g-values are consistent with the values from the EPR spectroscopy for complexes **10** and **11** (g = 2.12 for **10** in Figure S23 and g = 2.11 for **11** in Figure S24). Attempts to fit the susceptibility data in χ versus T to 2K have been made, however, the results are not well fit the experimental data, for example, the obtained g-values are largely deviated from the experimental g-values from the EPR spectra, and the molar fractions of noncoupled species are too high. This may be due to the combined presence of intramolecular antiferromagnetic coupling, inter-cluster interaction and/or spin-orbit coupling of low-spin Fe^{III} ions of **8** and **9** between 2- 60 K.[27] The plot of $M/N\beta$ vs H (M = magnetization) for samples **8** and **9** was measured at 2.0 K in the field range from -80K to +80K Oe in Figure S25. **8** and **9** showed characteristic antiferromagnetic behavior that the $M_{mol}/N\beta$ values increased gradually and slightly, as the magnetic field increased from 0 to 80K Oe.

By comparison of magnetic coupling constants of **8-11** with that of the analogous cis-Ru^{II}(bpy)$_2$(CN)$_2$ bridged complex (-13.6 cm^{-1}),[8] it can be found that the magnetic coupling strength between the distant paramagnetic Fe^{III} ions across diamagnetic cyanidometal NC-M^{II}-CN (M = Fe, Ru, Os) bridge increases with the central metal in the order of Fe < Ru < Os. This order is consistent with the increasing radial extension of the d orbitals and the degree of electron density delocalization over the cyanide group from Fe to Ru and then to Os.

Experimental Section

General Procedures and Materials

All manipulations were performed under argon atmosphere with the use of standard Schlenk techniques unless otherwise stated. Dichloromethane was dried by distillation over calcium hydride and diethyl-ether was dried by distillation over sodium wire under argon atmosphere. Methanol was dried by distillation over magnesium and acetonitrile was dried by distillation over calcium hydride under argon atmosphere. cis-Os^{II}(bpy)$_2$(CN)$_2$·7H$_2$O[17], cis-Os^{II}(phen)$_2$(CN)$_2$[28], cis-

$Fe^{II}(bpy)_2(CN)_2 \cdot 3H_2O^{29}$, cis-$Fe^{II}(phen)_2(CN)_2 \cdot 2H_2O^{29}$, and $CpFe^{II}(dppe)(NCCH_3)Br^{30}$ were prepared according to the literature procedures. All other reagents were available commercially and used without further purification.

5 **cis-[Cp(dppe)Fe^{II}(NC)Os^{II}(bpy)$_2$(CN)Fe^{II}(dppe)Cp][PF$_6$]$_2$ ·2C$_4$H$_{10}$O·CH$_2$Cl$_2$, 1·2Et$_2$O·CH$_2$Cl$_2$**

Under argon atmosphere, Cp(dppe)Fe^{II}(NCCH$_3$)Br (228 mg, 0.356 mmol) was added to a brown solution of cis-Os^{II}(bpy)$_2$(CN)$_2$·7H$_2$O (115 mg, 0.169 mmol) in methanol (10

10 ml) at room temperature. The reaction mixture was refluxed for 6 h, resulting in a red solution. NH$_4$PF$_6$ (60.8 mg, 0.373 mmol) was then added to the above reaction solution. A red precipitate appeared immediately and was collected. Deep red needle crystals **1** (122 mg, 34%) suitable for single-crystal X-ray

15 diffraction analysis were obtained from a mixed solution of dichloromethane and ethyl-ether (1:3, 40 ml). Anal. Calcd for OsFe$_2$C$_{84}$H$_{74}$N$_6$P$_6$F$_{12}$·2C$_4$H$_{10}$O·CH$_2$Cl$_2$: C, 52.78; H, 4.57; N, 3.97%. Found: C, 52.62; H, 4.03; N, 4.53%. IR (v_{CN}, KBr pellet, cm^{-1}): 2074. UV-vis (CH$_3$CN), λ_{max}, nm (ε, dm^3 mol^{-1} cm^{-1}): 387

20 (3412), 500 (4483), 695 (810). MS, m/z: 519.4 [Cp(dppe)Fe^{II}]$^+$, 1072.3 [**1** -Cp(dppe)Fe^{II}-2PF$_6$]$^+$, 1736.9 [**1**-PF$_6$]$^+$.

cis-[Cp(dppe)Fe^{III}(NC)Os^{II}(bpy)$_2$(CN)Fe^{II}(dppe)Cp][PF$_6$]$_3$, 5

To a solution of **1** (100 mg, 0.053 mmol) in dichloromethane (10 ml), Cp$_2$Fe^{III}(PF$_6$) (17.5 mg, 0.053 mmol) was added at room

25 temperature. The mixture was stirred at 30°C for 3 h and concentrated to 2 ml under reduced pressure, and then diethyl ether (20 ml) was added and a brown precipitate was obtained (90.3 mg, 84%). Anal. Calcd for OsFe$_2$C$_{84}$H$_{74}$N$_6$P$_7$F$_{18}$: C, 49.74; H, 3.68; N, 4.14%. Found: C, 49.70; H, 3.99; N, 4.14%. IR (v_{CN},

30 KBr pellet, cm^{-1}): 2074, 1992. UV-vis (CH$_3$CN), λ_{max}, nm (ε, dm^3 mol^{-1} cm^{-1}): 402 (6176), 910 (1731). MS, m/z: 519.1 [Cp(dppe)Fe^{II}]$^+$, 1073.3 [**5**-3PF$_6$-Cp(dppe)Fe^{III}]$^+$, 1882.0 [**5**-PF$_6$]$^+$.

cis-[Cp(dppe)Fe^{III}(NC)Os^{II}(bpy)$_2$(CN)Fe^{III}(dppe)Cp][PF$_6$]$_4$ ·3CH$_3$CN, 8·3CH$_3$CN

35 To a solution of **5** (100.0 mg, 0.049 mmol) in dichloromethane (10 ml), AgPF$_6$ (12.4 mg, 0.049 mmol) was added at room temperature. The solution immediately turned to brown and was stirred for another 3 h at 30°C and concentrated under a reduced pressure to obtain a black brown precipitate. The black brown

40 precipitate was collected, and washed with a little dichloromethane and ethyl ether. Deep brown prism crystals of **8** (47.3 mg, 42%) suitable for single crystal X-ray diffraction analysis were grown by layering diethyl ether (30ml) on the acetonitrile (10 ml) solution of the precipitate at room

45 temperature in the dark. Anal. Calcd for OsFe$_2$C$_{84}$H$_{74}$N$_6$P$_8$F$_{24}$·CH$_3$CN: C, 46.65; H, 3.50; N, 4.43%. Found: C, 46.65; H, 3.88; N, 4.52%. IR (v_{CN}, KBr pellet, cm^{-1}): 2039, 1987. UV-vis (CH$_3$CN), λ_{max}, nm (ε, dm^3 mol^{-1} cm^{-1}): 383 (9256), 402 (9264), 896 (3463). MS, m/z: 1218.8 [**8**-3PF$_6$-

50 Cp(dppe)Fe^{III}]$^+$, 2026.4 [**8**-PF$_6$]$^+$.

cis-[Cp(dppe)Fe^{II}(NC)Os^{II}(phen)$_2$(CN)Fe^{II}(dppe)Cp][PF$_6$]$_2$ ·4CH$_2$Cl$_2$, 2·4CH$_2$Cl$_2$

The preparation of compound **2** was similar to that described method for compound **1**, but cis-Os^{II}(phen)$_2$(CN)$_2$ (100 mg, 0.166 mmol),

55 Cp(dppe)Fe^{II}(NCCH$_3$)Br (223 mg, 0.349 mmol) and NH$_4$PF$_6$

(59.5 mg, 0.365 mmol) were used, yielding **2** as red needle crystals (102 mg, 27%). Anal. Calcd for OsFe$_2$C$_{88}$H$_{74}$N$_6$P$_6$F$_{12}$·CH$_2$Cl$_2$: C, 53.02; H, 3.80; N 4.17%. Found: C, 53.04; H, 4.38; N, 4.35%. IR (v_{CN}, KBr pellet, cm^{-1}): 2072.

60 UV-vis (CH$_3$CN), λ_{max}, nm (ε, dm^3 mol^{-1} cm^{-1}): 385 (12739), 464 (8378), 507 (8643), 692 (2204). MS, m/z: 520.1 [Cp(dppe)Fe^{II}]$^+$, 1121.4 [**2**-2PF$_6$-Cp(dppe)Fe^{II}]$^+$, 1784.7 [**2**-PF$_6$]$^+$.

cis-[Cp(dppe)Fe^{III}(NC)Os^{II}(phen)$_2$(CN)Fe^{II}(dppe)Cp][PF$_6$]$_3$, 6

The preparation of compound **6** was similar to that described method

65 for compound **5**, but **2** (100 mg, 0.052 mmol) and Cp$_2$Fe^{III}(PF$_6$) (17.2 mg, 0.052 mmol) was used, yielding **6** as brown prism crystals (42.1 mg, 39%). Anal. Calcd for OsFe$_2$C$_{88}$H$_{74}$N$_6$P$_7$F$_{18}$: C, 50.91; H, 3.59; N, 4.05%. Found: C, 50.37; H, 3.71; N, 4.07%. IR (v_{CN}, KBr pellet, cm^{-1}): 2072, 1993. UV-vis (CH$_3$CN), λ_{max},

70 nm (ε, dm^3 mol^{-1} cm^{-1}): 386 (9800), 406 (9777), 625 (1326), 912 (1326). MS, m/z: 519.3 [Cp(dppe)Fe^{II}]$^+$, 1123 [**6**-3PF$_6$-Cp(dppe)Fe^{III}]$^+$, 1267.9 [**6**-2PF$_6$-Cp(dppe)Fe^{II}]$^+$, 1931.3 [**6**-PF$_6$]$^+$.

cis-[Cp(dppe)Fe^{III}(NC)Os^{II}(phen)$_2$(CN)Fe^{III}(dppe)Cp][PF$_6$]$_4$·CH$_3$CN, 9·CH$_3$CN

75 The preparation of compound **9** was similar to that described procedure for compound **8**, but **6** (100 mg, 0.048 mmol) and AgPF$_6$ (12.1 mg, 0.048 mmol) was used, yielding **9** as brown prism crystals (32.6 mg, 30%). Anal. Calcd for OsFe$_2$C$_{88}$H$_{74}$N$_6$P$_8$F$_{24}$: C, 47.58; H, 3.36; N, 3.78%. Found: C,

80 47.17; H, 3.90; N, 3.82%. IR (v_{CN}, KBr pellet, cm^{-1}): 2042, 1993. UV-vis (CH$_3$CN), λ_{max}, nm (ε, dm^3 mol^{-1} cm^{-1}): 404 (9036), 886 (3036). MS, m/z: 1266.9 [**9**-3PF$_6$-Cp(dppe)Fe^{III}]$^+$, 2075.2 [**9**-PF$_6$]$^+$.

cis-[Cp(dppe)Fe^{II}(NC)Fe^{II}(bpy)$_2$(CN)Fe^{II}dppe)Cp][PF$_6$]$_2$· 2CH$_2$Cl$_2$·C$_4$H$_{10}$O, 3·2CH$_2$Cl$_2$·C$_4$H$_{10}$O

85 This complex was prepared according to a modified method based on the previous report,[15] but cis-Fe^{II}(bpy)$_2$(CN)$_2$ (100 mg, 0.211 mmol), Cp(dppe)Fe^{II}(NCCH)Br (284 mg, 0.443 mmol) and NH$_4$PF$_6$ (75.6 mg, 0.464 mmol) were used, yielding **3** as gray

90 prism crystals (147 mg, 35%). Anal. Calcd for C$_{84}$H$_{74}$F$_{12}$Fe$_3$N$_6$P$_6$: C, 57.69; H, 4.26; N, 4.81%. Found: C, 58.42; H, 4.46; N, 5.25%. IR (v_{CN}, KBr pellet, cm^{-1}): 2094. λ_{max}, nm (ε, dm^3 mol^{-1} cm^{-1}): 372 (2706), 517 (1826), 563 (2095). MS, m/z: 519.4 [Fe(dppe)Cp]$^+$, 939.2 [**3** - Fe^{II}(dppe)Cp -2PF$_6$]$^+$, 1603.0 [**3** -PF$_6$]$^+$

95 **cis-[Cp(dppe)Fe^{III}(NC)Fe^{II}(bpy)$_2$(CN)Fe^{III}(dppe)Cp][PF$_6$]$_4$ ·3CH$_3$CN, 10·3CH$_3$CN**

This complex was prepared according to a modified method based on the previous report,[15] but **3** (100 mg, 0.057 mmol) and Cp$_2$Fe^{III}(PF$_6$) (37.7 mg, 0.114 mmol) was used, yielding **10** as red

100 prism crystals (48.1 mg, 39%). Anal. Calcd for C$_{84}$H$_{74}$F$_{24}$Fe$_3$N$_6$P$_8$: C, 49.49; H, 3.66; N, 4.12%. Found: C, 49.45; H, 4.14; N, 3.63%. IR (v_{CN}, KBr pellet, cm^{-1}): 2035. λ_{max}, nm (ε, dm^3 mol^{-1} cm^{-1}): 489 (6506), 1210 (2987). MS, m/z: 1893.3[**10**-PF$_6$].

105 **cis-[Cp(dppe)Fe^{III}(NC)Fe^{II}(phen)$_2$(CN)Fe^{II}(dppe)Cp][PF$_6$]$_2$·4 CH$_2$Cl$_2$, 4·4CH$_2$Cl$_2$**

The preparation of compound **4** was similar to that described method for compound **3**, cis-Fe^{II}(phen)$_2$(CN)$_2$ (100 mg, 0.198 mmol), Cp(dppe)Fe^{II}(NCCH$_3$)Br (279 mg, 0.436 mmol) and NH$_4$PF$_6$

(71.0 mg, 0.436 mmol) were used, yielding **4** as gray prism crystals (97.3 mg, 23%). Anal. Calcd for $C_{88}H_{74}F_{12}Fe_3N_6P_6 \cdot CH_2Cl_2$: C, 53.27; H, 3.93; N, 4.10%. Found: C, 52.90; H, 3.88; N, 4.89%. IR (ν_{CN}, KBr pellet, cm^{-1}): 2094.

5 UV-vis (CH$_3$CN), λ_{max}, nm (ε, dm^3 mol^{-1} cm^{-1}): 378 (3717), 504 (7797), 553 (8465). MS m/z: 519.7 [Fe^{II}(dppe)Cp]$^+$, 987.2 [**4**-2PF$_6$-Fe^{II}(dppe)Cp]$^+$, 1651.1 [**4**-PF$_6$]$^+$.

cis-[Cp(dppe)Fe^{III}(NC)Fe^{II}(phen)$_2$(CN)Fe^{II}(dppe)Cp][PF$_6$]$_3$· 0.5C$_4$H$_{10}$O·0.5H$_2$O, 7·0.5C$_4$H$_{10}$O·0.5H$_2$O

10 The preparation of compound **7** was similar to that described procedure for compound **5**, but **4** (100 mg, 0.056 mmol) and Cp$_2$Fe^{III}(PF$_6$) (18.6 mg, 0.056 mmol) was used, yielding **7** as brown prism crystals (39.4 mg, 34%). Anal. Calcd for Anal. Calcd for $C_{88}H_{74}F_{18}Fe_3N_6P_7$: C, 54.43; H, 3.84; N, 4.33%. Found:

15 C, 53.89; H, 3.91; N, 4.33%. IR (ν_{CN}, KBr pellet, cm^{-1}): 2094, 2033. UV-vis (CH$_3$CN), λ_{max}, nm (ε, dm^3 mol^{-1} cm^{-1}): 502 (4035), 572 (2246), 1217 (1372). MS, m/z: 519.6 [Fe^{II}(dppe)Cp]$^+$, 987.1 [**7**-3PF$_6$-Fe^{III}(dppe)Cp]$^+$, 1131.8 [**7**-Cp^{II}Fe(dppe)-2PF$_6$]$^+$, 1796.4 [**7**-PF$_6$]$^+$.

20 *cis*-[Cp(dppe)Fe^{III}(NC)Fe^{II}(phen)$_2$(CN)Fe^{III}(dppe)Cp][PF$_6$]$_4$, 11

The preparation of compound **11** was similar to that described procedure for compound **8**, but **7** (100 mg, 0.052 mmol) and Cp$_2$Fe^{III}(PF$_6$) (17.2 mg, 0.052 mmol) was used, yielding **11** as brown solid (80.3 mg, 74%). Anal. Calcd for $C_{88}H_{74}F_{24}Fe_3N_6P_8$:

25 C, 50.65; H, 3.57; N, 4.03%. Found: C, 50.15; H, 3.46; N, 4.08%. IR (ν_{CN}, KBr pellet, cm^{-1}): 2032. UV-vis (CH$_3$CN), λ_{max}, nm (ε, dm^3 mol^{-1} cm^{-1}): 470 (4873), 494 (4917), 1172 (2730). MS m/z: 1131.9 [**11**-Cp^{III}Fe(dppe)-3PF$_6$]$^+$, 1940.1 [**11**-PF$_6$]$^+$.

30 **Physical measurements**

Elemental analyses (C, H, N) were performed at a Vario MICRO elemental analyzer. Mass spectra (MS) were collected on DECAX-3000 LCQ Deca XP Ion Trap mass spectrometer using acetonitrile as the mobile phase. Infrared (IR) spectra were

35 obtained from KBr pellets with a Perkin-Elmer Spectrum One spectrophotometer. Electrochemical measurements were performed under an argon atmosphere using V3-Studio in acetonitrile solution with 0.1 M (Bu$_4$N)(PF$_6$) as a supporting electrolyte at a scan rate of 100 mV s^{-1} by cyclic voltammetry

40 (CV). Glassy graphite and platinum were used as the working and counter electrodes, respectively, and the potentials were measured against 3 M KCl Ag/AgCl as reference electrode. UV-vis-NIR spectra were measured on a Perkin-Elmer Lambda 900 UV-vis-NIR spectrophotometer. The various temperature

45 magnetic susceptibilities of the polycrystalline samples were carried out using a Magnetic Property Measurement System MPMS SQUID-XL under an applied magnetic field of 1000 Oe in a 2-300 K temperature range. The isothermal magnetisation measurements were conducted on a Physical Property

50 Measurement System (PPMS) PPMS-9T. Diamagnetic corrections were made using Pascal's constants. EPR spectra were recorded on the samples at room temperature with a Bruker ELEXSYS E500 spectrometer.

X-Ray structure determination

55 The single crystal data of complexes **1-4** and **6-10** were all collected on Saturn724+ diffractometer equipped with graphite-monochromatic Mo K_α ($\lambda = 0.71073$ Å) radiation using an ω scan mode at 123 K. The structures were solved by direct methods and refined using the *SHELXL-97* program suite.[31] Hydrogen atoms

60 were calculated geometrically and refined using a riding model. Anisotropic thermal parameters were used for the non-hydrogen atoms, and isotropic parameters were used for the hydrogen atoms. All non-hydrogen atoms were refined by full-matrix least-squares on F^2. The R values are defined as $_\omega R_1 = \Sigma||F_o| - |F_c||/\Sigma|F_o|$

65 and $_\omega R_2 = [\Sigma[\omega(F_o^2 - F_c^2)^2]/\Sigma[\square \omega(F_o^2)^2]]^{1/2}$. The detailed crystal data for complexes **1-3** are summarized in Table S1, and complexes **4** and **6-10** are summarized in Table 1. Selected bond lengths and angles for complexes **1-3** are presented in Table S2, and complexes **4** and **6-10** are given in Table 2.

70 CCDC- 1031311 (**1**), CCDC-1031312 (**8**), CCDC- 1031313 (**2**), CCDC-1031314 (**6**), CCDC-1031315 (**9**), CCDC-1037810 (**3**), CCDC-1037811 (**10**), CCDC-1041440 (**4**) and CCDC-1041441 (**7**) contain the supplementary crystallographic data, related bond lengths and angles for this paper.

75 **Conclusions**

In summary, tri-nuclear complexes **1-4** and their oxidized species **5-11** were synthesized and fully characterized. Moreover, the crystals of **1-4** and **6-10** suitable for single-crystal X-ray diffraction analysis were obtained. The maximum absorption

80 wavelengths in the NIR region of the one-electron oxidation mixed-valence complexes **5-7** are assigned to the mixture of the central M^{II}→terminal Fe^{III} and terminal Fe^{II}→ terminal Fe^{III} MMCTs. Whereas, those in the NIR region of the two-electron oxidation products **8-11** are assigned to the central M^{II}→terminal

85 Fe^{III} MMCT. And the energy increases with the central metal in the order of Fe < Os < Ru in the two oxidized products. The two-electron oxidation products (**8** and **9**) with NC-Os^{II}(L)$_2$-CN bridge exhibit a strong antiferromagnetic coupling between the two distant Fe^{III} ions although separated by the diamagnetic

90 cyanidometal NC-Os^{II}(L)$_2$-CN bridge ($J = -25.8$ and -26.1 cm^{-1}). To the best of our knowledge, this is the strongest magnetic coupling between the distant paramagnetic metal ions across a diamagnetic cyanidometal bridge reported by far. For the two-electron oxidation products (**10** and **11**) with the diamagnetic NC-

95 Fe^{II}(L)$_2$-CN bridge, however, the distant two Fe^{III} ions posses only very weak antiferromagnetic coupling ($J = -0.15$ and -0.19 cm^{-1}). The magnetic susceptibilities studies indicate the magnetic coupling strength between the distant paramagnetic Fe^{III} ions across diamagnetic cyanidometal NC-M^{II}-CN (M = Fe, Ru, Os)

100 bridge increases with the central metal in the order of Fe < Ru < Os. More importantly, this work reveals that for the investigated system the distant magnetic interaction strength is directly associated with the degree of electron density delocalization over the cyanide groups in the central diamagnetic cyanidometal.

Table 1. Crystallographic Data and Details of Structure Determination for **4** and **6-10**.

	4·4CH₂Cl₂	**6**	**7·0.5Et₂O·0.5H₂O**
Chemical formula	$C_{92}H_{82}Cl_8F_{12}Fe_3N_6P_6$	$C_{88}H_{74}F_{18}Fe_2N_6OsP_7$	$C_{94}H_{86}F_{18}Fe_2N_8OP_7$
Formula weight	2136.61	2076.22	2070.05
Colour and Habit	Gray prism	Brown prism	Brown prism
Crystal Size / mm	0.44×0.40×0.18	0.42×0.14×0.12	0.52×0.38×0.08
T / K	123	123	123
Crystal system	Orthorhombic	Monoclinic	Monoclinic
Space group	$Pbca$	$P2_1/c$	$P2_1/c$
a / Å	28.122(7)	12.768(7)	12.464(5)
b /Å	19.966(5)	32.866(18)	33.789(11)
c / Å	33.171(8)	23.450(12)	23.650(6)
α / °	90.00	90.00	90.00
β / °	90.00	114.20(2)	113.419(15)
γ / °	90.00	90.00	90.00
V / Å³	18625(8)	8976(8)	9140(5)
Z	8	4	4
ρ_{calcd}(g/cm³)	1.524	1.536	1.504
λ (Mo K_α, Å)	0.71073	0.71073	0.71073
μ(Mo K_α, mm⁻¹)	0.868	1.941	0.682
Completeness	99.8%	99.3%	95.9%
$F(000)$	8704	4156	4236
h, k, l, range	-34≤h≤36, -25≤k≤25, -43≤l≤43	-15≤h≤15, -39≤k≤39, -27≤l≤27	-14≤h≤14, -40≤k≤40, -27≤l≤28
θ range / deg	2.13-27.50	2.08-25.00	2.04-25.00
Reflections measured	21331	15693	15428
R_{int}	0.0883	0.0878	0.0556
Params/restraints/Data(obs.)	1234/99/ 17573	1099/48/12194	1315/433/ 12060
GOF	1.080	1.100	1.083
$R_1, {}_\omega R_2$ ($I >2\ \sigma(I)$)	0.0782, 0.2015	0.0918, 0.2208	0.0778, 0.1988
$R_1, {}_\omega R_2$ (all data)	0.0921, 0.2177	0.1139, 0.2449	0.0926, 0.2192

Complex	**8·3CH₃CN**	**9·CH₃CN**	**10·3CH₃CN**
Chemical formula	$C_{90}H_{83}F_{24}Fe_2N_9OsP_8$	$C_{90}H_{77}F_{24}Fe_2N_7OsP_8$	$C_{90}H_{83}F_{24}Fe_3N_9P_8$
Formula weight	2296.31	2262.25	2161.96
Colour and Habit	Brown prism	Brown prism	Brown prism
Crystal Size / mm	0.85×0.50×0.45	0.62×0.36×0.17	0.70×0.42×0.38
T / K	123	123	123
Crystal system	Monoclinic	Monoclinic	Monoclinic
Space group	$P2_1/c$	$P2_1/c$	$P2_1/c$
a / Å	17.0424(10)	17.461(3)	17.0101(5)
b /Å	20.3140(7)	22.961(4)	20.1743(4)
c / Å	28.6650(15)	23.660(4)	28.6493(9)
α / °	90.00	90.00	90.00
β / °	97.699(3)	107.212(3)	97.160(2)
γ / °	90.00	90.00	90.00
V / Å³	9834.3(8)	9061(3)	9754.8(5)
Z	4	4	4
ρ_{calcd}(g/cm³)	1.551	1.658	1.472
λ (Mo K_α, Å)	0.71073	0.71073	0.71073
μ(Mo K_α, mm⁻¹)	1.804	1.956	0.666
Completeness	99.1%	99.4%	98.7%
$F(000)$	4600	4520	4400
h, k, l, range	-22≤h≤22, -26≤k≤26, -37≤l≤37	-22≤h≤22, -28≤k≤29, -30≤l≤30	-22≤h≤22, -25≤k≤25, -37≤l≤37
θ range / deg	2.01-27.52	2.06-27.47	2.23-27.48
Reflections measured	22456	20650	22081
R_{int}	0.0671	0.0594	0.0381
Params/restraints/Data(obs.)	1298/164/19545	1279/332/17833	1391/549/19744
GOF	1.068	1.089	1.041
$R_1, {}_\omega R_2$ ($I >2\ \sigma(I)$)	0.0493, 0.1213	0.0666, 0.1469	0.0611, 0.1666
$R_1, {}_\omega R_2$ (all data)	0.0586, 0.1277	0.0779, 0.1546	0.0685, 0.1731

${}_\omega R_1 = \Sigma ||F_o| - |F_c||/\Sigma|F_o|$ and ${}_\omega R_2 = [\Sigma[\omega(F_o^2 - F_c^2)^2]/\Sigma[\square\ \omega(F_o^2)^2]]^{1/2}$

Table 2. Selected Bond Distances (Å) and Bond Angles (°) for **4** and **6-10**.

	6	**8**	**9**
Os-C1	1.966(10)	1.950(4)	1.950(6)
Os-C2	1.912(11)	1.953(4)	1.957(6)
Os-N3	2.137(9)	2.122(3)	2.134(4)
Os-N4	2.084(8)	2.078(3)	2.078(5)
Os-N5	2.105(8)	2.075(3)	2.084(4)
Os-N6	2.102(9)	2.117(3)	2.136(4)
C1≡N1	1.179(13)	1.163(5)	1.165(7)
C2≡N2	1.218(13)	1.160(5)	1.171(7)
Fe1-N1	1.928(8)	1.885(3)	1.875(5)
Fe2-N2	1.879(8)	1.878(3)	1.888(5)
Fe1-P1	2.205(3)	2.268(1)	2.266 (2)
Fe1-P2	2.200(3)	2.245(1)	2.271(2)
Fe2-P3	2.254(3)	2.261(1)	2.254(2)
Fe2-P4	2.252(3)	2.252(1)	2.250(2)
C1-Os-C2	93.4(4)	95.8(2)	94.5(2)
N1≡C1-Os	175.4(9)	172.9(3)	171.9(5)
N2≡C2-Os	177.6(8)	172.1(3)	176.5(5)
C1≡N1-Fe1	179.6(9)	172.1(3)	177.6(5)
C2≡N2-Fe2	176.8(7)	176.9(3)	173.3(5)
Os···Fe1	5.073	4.977	4.974
Os···Fe2	5.009	4.977	5.001
Fe1···Fe2	7.618	7.953	7.881
Fe1···Fe2(-NC-Os-CN)	10.082	9.989	10.006

	4	**7**	**10**
Fe3-C1	1.904(4)	1.865(5)	1.879(3)
Fe3-C2	1.916(4)	1.908(5)	1.874(3)
Fe3-N3	2.007(3)	2.008(4)	2.002(3)
Fe3-N4	1.976(3)	1.974(4)	1.969(3)
Fe3-N5	1.967(3)	1.973(4)	1.980(3)
Fe3-N6	1.999(3)	1.997(4)	1.996(3)
C1≡N1	1.165(5)	1.183(6)	1.165(4)
C2≡N2	1.162(5)	1.182(7)	1.164(4)
Fe1-N1	1.920(3)	1.888(4)	1.905(3)
Fe2-N2	1.921(3)	1.910(4)	1.893(2)
Fe1-P1	2.194(1)	2.261(2)	2.253(1)
Fe1-P2	2.200(1)	2.265(2)	2.272(1)

Fe2-P3	2.191(1)	2.208(2)	2.267(1)
Fe2-P4	2.203(1)	2.196(2)	2.256(1)
C1-Fe3-C2	91.8(2)	94.0(2)	95.7(3)
N1≡C1-Fe3	176.7(3)	175.2(4))	173.1(3)
N2≡C2-Fe3	174.3(3)	173.4(4)	172.6(3)
C1≡N1-Fe1	179.6(4)	174.9(4)	173.7(2)
C2≡N2-Fe2	177.5(3)	178.0(4)	178.8(3)
Fe3···Fe1	4.989	4.921	4.929
Fe3··Fe2	4.999	4.992	4.919
Fe1····Fe2	7.436	7.697	7.867
Fe1···Fe2(-NC-Fe-CN)	9.988	9.936	9.880

Table 3 Cyanide Stretching Frequencies, Electronic Absorption Spectra and Cyclic-Voltammetry Data for Complex **1-11**.

	ν_{CN} (cm^{-1})	λ_{max}, nm (ε, dm^3 mol^{-1} cm^{-1})	P (V)
12A[a]	2040, 2057	336(11870), 372(11569), 445(10667), 496(13074), 650(3370)	0.47
12B[a]	2053, 2067	346(9428), 483(10385)	0.86
12C[a]	2069, 2079	382(6252),581(6204)	0.46
1	2074	387(3412), 500(4483), 695(810)	
5	2074, 1992	402 (6176), 910 (1731)	0.22,0.39
8	2039, 1987	383 (9256), 402 (9264), 896 (3463)	
2	2072	385 (12739), 464 (8378), 507 (8643), 692 (2204).	
6	2072, 1993	386 (9800), 406(9777), 625 (1326), 912 (1326)	0.22 0.38
9	2042, 1993	404(9036), 886(3036)	
13A[b]	2086	362 (7253), 480(5620).	
13B	2094, 2020	389(7465), 791(5460)	0.25, 0.36
13C[b]	2059, 2021	391(8363), 722 (8238).	
14A[c]	2089	380 (7169), 466 (8088).	
14B[c]	2092, 2019	371 (10479), 777 (5238)	0.26, 0.37
14C[c]	2063, 2062	350 (10658), 717 (8416)	
3	2094	372 (2706), 517 (1826), 563 (2095)	0.29, 0.41
10	2035	489 (6506), 1210 (2987)	
4	2094	378 (3717), 504 (7797), 553 (8465)	0.28, 0.40
7	2094, 2033	502 (4035), 572 (2246), 1217 (1372)	
11	2032	470 (4873), 494 (4917), 1172 (2730)	

a: 12A, 12B and 12C represent *cis*-M(bpy)$_2$(CN)$_2$ (M = Os, Ru, Fe), respectively, see reference[17, 18]

b: 13A, 13B and 13C represent *cis*-[Cp(dppe)Fe^{II}(NC)Ru^{II}(bpy)$_2$(CN)Fe^{II}(dppe) Cp](PF$_6$)$_2$ and its one-electron and two-electron oxidation products, respectively, see reference[7]

c: 14A, 14B and 14C represent *cis*-[Cp(dppe)Fe^{II}(NC)Ru^{II}(phen)$_2$(CN)Fe^{II}(dppe) Cp](PF$_6$)$_2$ and its one-electron and two-electron oxidation products, respectively, see reference[8]
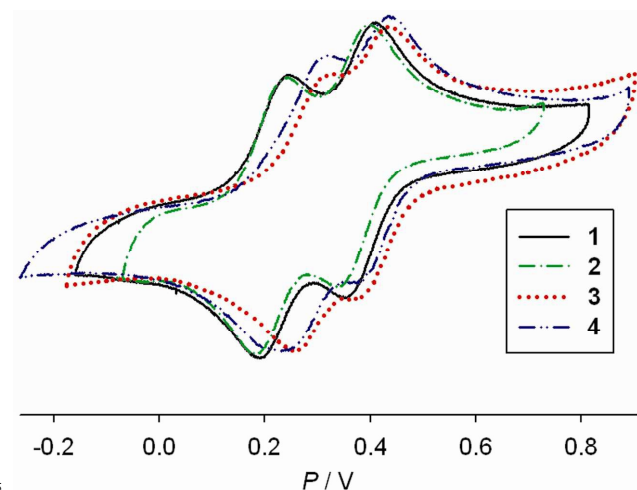
Figure 1. Cyclic voltammogram of complexes **1-4** in a 0.10 M acetonitrile solution of [Bu$_4$N][PF$_6$] at a scan rate of 100 mV s^{-1}.
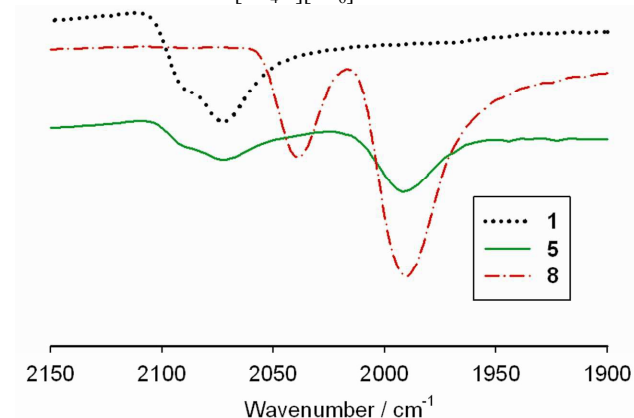
Figure 2. IR spectra of complexes **1, 5** and **8** at room temperature (KBr pellet).
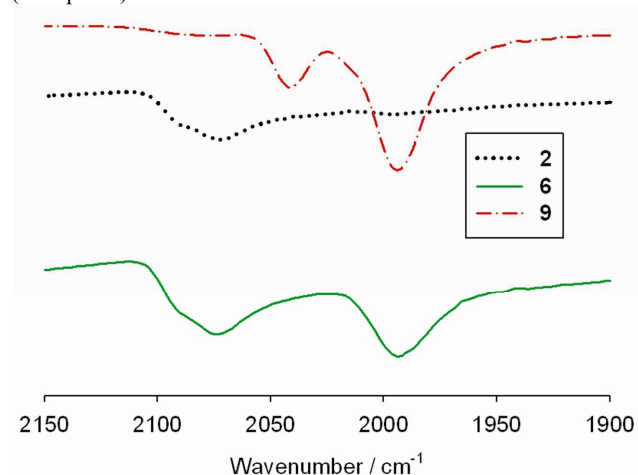
Figure 3. IR spectra of complexes **2**, **6** and **9** at room temperature (KBr pellet).
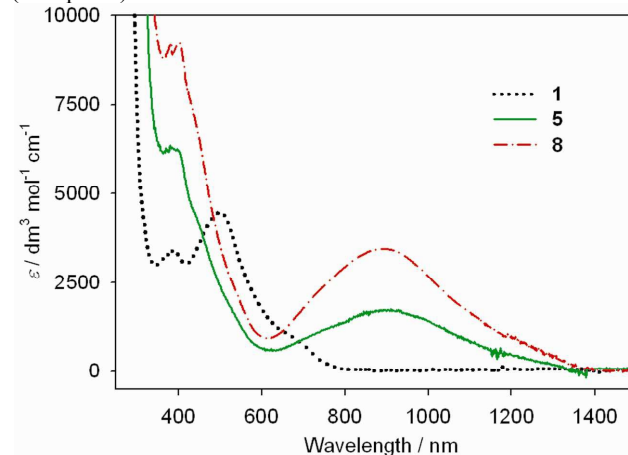
Figure 4. Electronic absorption spectra of complexes **1, 5** and **8** in CH$_3$CN at room temperature.
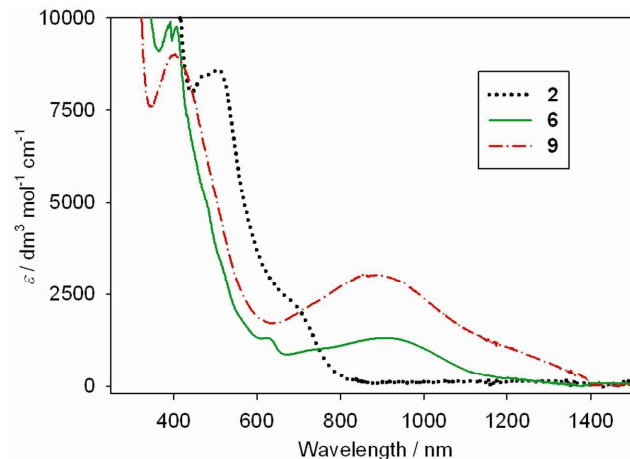
Figure 5. Electronic absorption spectra of complexes **2**, **6** and **9** in CH$_3$CN at room temperature.
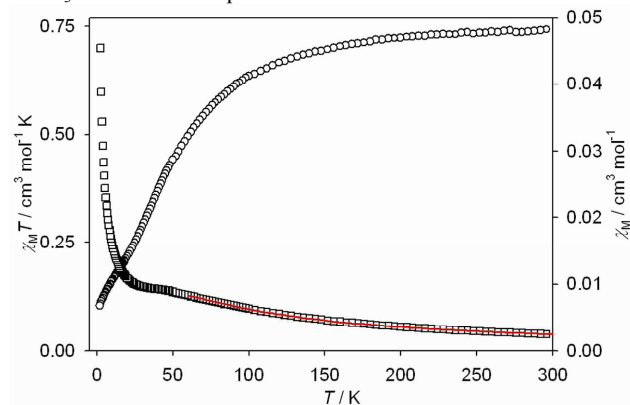
5 **Figure 6.** Magnetic behavior of complex **8** as measured in an applied field of 1000 Oe using a SQUID magnetometer. Fitting (red line) on χ_M vs T (square) and $\chi_M T$ vs T (circle) of complex **8** in polycrystalline sample.
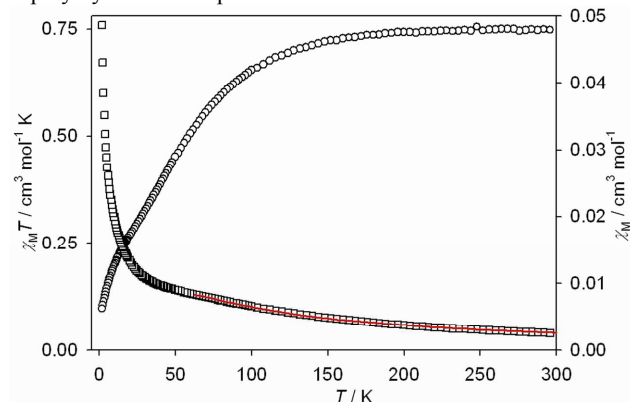
10 **Figure 7.** Magnetic behavior of complex **9** as measured in an applied field of 1000 Oe using a SQUID magnetometer. Fitting (red line) on χ_M vs T (square) and $\chi_M T$ vs T (circle) of complex **9** in polycrystalline sample.
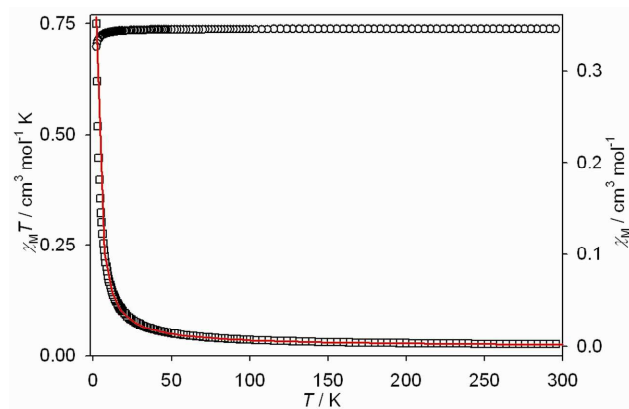
15 **Figure 8.** Magnetic behavior of complex **10** as measured in an applied field of 1000 Oe using a SQUID magnetometer. Fitting (red line) on χ_M vs T (square) and $\chi_M T$ vs T (circle) of complex **10** in polycrystalline sample.
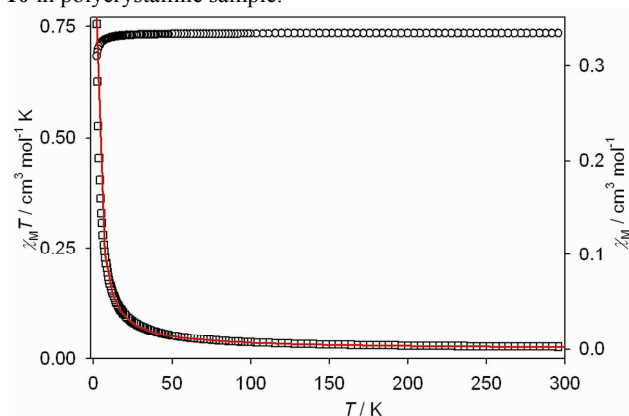
20 **Figure 9.** Magnetic behavior of complex **10** as measured in an applied field of 1000 Oe using a SQUID magnetometer. Fitting (red line) on χ_M vs T (square) and $\chi_M T$ vs T (circle) of complex **10** in polycrystalline sample.

25 **Notes and references**

State Key Laboratory of Structure Chemistry, Fujian Institute of Research on the Structure of Matter, Chinese Academy of Sciences, Fuzhou, 350002, China. E-mail: tsheng@fjirsm.ac.cn.
‡ Footnotes should appear here. These might include comments relevant to but not central to the matter under discussion, limited experimental and spectral data, and crystallographic data.

35
1. A. Dei, *Angew. Chem. Int. Ed.*, 2005, **44**, 1160; V. Escax, G. Champion, M. A. Arrio, M. Zacchigna, C. C. D. Moulin and A. Bleuzen, *Angew. Chem. Int. Ed.*, 2005, **44**, 4798; J. M. Herrera, V. Marvaud, M. Verdaguer, J. Marrot, M. Kalisz and C. Mathoniere, 40 *Angew. Chem. Int. Ed.*, 2004, **43**, 5468; H. Svendsen, J. Overgaard, M. Chevallier, E. Collet and B. B. Iversen, *Angew. Chem. Int. Ed.*, 2009, **48**, 2780; R. Ababei, C. Pichon, O. Roubeau, Y.-G. Li, N. Bréfuel, L. Buisson, P. Guionneau, C. Mathonière and R. Clérac, *J. Am. Chem. Soc.*, 2013, **135**, 14840; J. D. Cafun, G. Champion, M. A. 45 Arrio, C. C. D. Moulin and A. Bleuzen, *J. Am. Chem. Soc.*, 2010, **132**, 11552; T. Hozumi, K. Hashimoto and S. Ohkoshi, *J. Am. Chem. Soc.*, 2005, **127**, 3864.
2. M. Verdaguer, A. Bleuzen, V. Marvaud, J. Vaissermann, M. Seuleiman, C. Desplanches, A. Sciuller, C. Train, R. Garde, G. Gelly, 50 C. Lomenech, I. Rosenman, P. Veillet, C. Cartier and F. Villain,

Coord. Chem. Rev., 1999, **192**, 1023; W. R. Entley and G. S. Girolami, *Science*, 1995, **268**, 397; T. Mallah, S. Thiebaut, M. Verdaguer and P. Veillet, *Science*, 1993, **262**, 1554; O. Sato, T. Iyoda, A. Fujishima and K. Hashimoto, *Science*, 1996, **271**, 49; S. Ferlay, T. Mallah, R. Ouahes, P. Veillet and M. Verdaguer, *Nature*, 1995, **378**, 701.

3. S. Wang, J. L. Zuo, H. C. Zhou, H. J. Choi, Y. X. Ke, J. R. Long and X. Z. You, *Angew. Chem. Int. Ed.*, 2004, **43**, 5940; L. M. C. Beltran and J. R. Long, *Acc. Chem. Res.*, 2005, **38**, 325; D. Li, S. Parkin, G. Wang, G. T. Yee, A. V. Prosvirin and S. M. Holmes, *Inorg. Chem.*, 2005, **44**, 4903; T. Glaser, M. Heidemeier, T. Weyhermuller, R. D. Hoffmann, H. Rupp and P. Muller, *Angew. Chem. Int. Ed.*, 2006, **45**, 6033; M. Atanasov, P. Comba, S. Hausberg and B. Martin, *Coord. Chem. Rev.*, 2009, **253**, 2306; K. S. Pedersen, M. Schau-Magnussen, J. Bendix, H. Weihe, A. V. Palii, S. I. Klokishner, S. Ostrovsky, O. S. Reu, H. Mutka and P. L. W. Tregenna-Piggott, *Chem.-Eur. J.*, 2010, **16**, 13458.

4. R. Lescoüezec, L. M. Toma, J. Vaissermann, M. Verdaguer, F. S. Delgado, C. Ruiz-Pérez, F. Lloret and M. Julve, *Coord. Chem. Rev.*, 2005, **249**, 2691; L. M. Toma, R. Lescouezec, J. Pasan, C. Ruiz-Perez, J. Vaissermann, J. Cano, R. Carrasco, W. Wernsdorfer, F. Lloret and M. Julve, *J. Am. Chem. Soc.*, 2006, **128**, 4842; S. Wang, J. L. Zuo, S. Gao, Y. Song, H. C. Zhou, Y. Z. Zhang and X. Z. You, *J. Am. Chem. Soc.*, 2004, **126**, 8900; M. X. Yao, Q. Zheng, K. Qian, Y. Song, S. Gao and J. L. Zuo, *Chem.-Eur. J.*, 2013, **19**, 294.

5. M. Steinert, B. Schneider, S. Dechert, S. Demeshko and F. Meyer, *Angew. Chem. Int. Ed.*, 2014, **53**, 6135; D. Y. Wu, O. Sato, Y. Einaga and C. Y. Duan, *Angew. Chem. Int. Ed.*, 2009, **48**, 1475; B. Schneider, S. Demeshko, S. Dechert and F. Meyer, *Angew. Chem. Int. Ed.*, 2010, **49**, 9274; M. Shatruk, A. Dragulescu-Andrasi, K. E. Chambers, S. A. Stoian, E. L. Bominaar, C. Achim and K. R. Dunbar, *J. Am. Chem. Soc.*, 2007, **129**, 6104; S.-i. Ohkoshi, K. Imoto, Y. Tsunobuchi, S. Takano and H. Tokoro, *Nat. Chem.*, 2011, **3**, 564.

6. X. Ma, S. M. Hu, C. H. Tan, Y. H. Wen, Q. L. Zhu, C. J. Shen, T. L. Sheng and X. T. Wu, *Dalton Trans.*, 2012, **41**, 12163.

7. X. Ma, S. M. Hu, C. H. Tan, Y. F. Zhang, X. D. Zhang, T. L. Sheng and X. T. Wu, *Inorg. Chem.*, 2013, **52**, 11343.

8. X. Ma, C. S. Lin, S. M. Hu, C. H. Tan, Y. H. Wen, T. L. Sheng and X. T. Wu, *Chem.-Eur. J.*, 2014, **20**, 7025.

9. Y. Wang, X. Ma, S. M. Hu, Y. L. Wang, C. H. Tan, Y. H. Wen, X. D. Zhang, T. L. Sheng and X. T. Wu, *Polyhedron*, 2014, **83**, 137; Y. Wang, J. S. Song, X. Ma, Z. Z. Xue, S. M. Hu, R. B. Fu, C. S. Li, T. L. Sheng and X. T. Wu, *RSC Adv.*, 2015, **5**, 3399.

10. G. Rogez, A. Marvilliers, E. Riviere, J. P. Audiere, F. Lloret, F. Varret, A. Goujon, N. Mendenez, J. J. Girerd and T. Mallah, *Angew. Chem. Int. Ed.*, 2000, **39**, 2885; D. Zhang, L. Zhang, Z. Zhao and Z. Ni, *Bull. Korean Chem. Soc.*, 2011, **32**, 2544; H. Oshio, M. Yamamoto and T. Ito, *Inorg. Chem.*, 2002, **41**, 5817; D. P. Zhang and P. Wang, *Inorg. Chem. Commun.*, 2012, **26**, 77; K. Halbauer, E. T. Spielberg, A. Sterzik, W. Plass and W. Imhof, *Inorg. Chim. Acta*, 2010, **363**, 1013; K. Halbauer, G. Leibeling and W. Imhof, *Z. Anorg. Allg. Chem.*, 2006, **632**, 264; H. Vahrenkamp, A. Gei and G. N. Richardson, *J. Chem. Soc., Dalton Trans.*, 1997, 3643; G. N. Richardson, U. Brand and H. Vahrenkamp, *Inorg. Chem.*, 1999, **38**, 3070; T. Sheng and H. Vahrenkamp, *Inorg. Chim. Acta*, 2004, **357**, 1739.

11. M. Shatruk, C. Avendano and K. R. Dunbar, in *Prog. Inorg. Chem.*, John Wiley & Sons, Inc., 2009, vol. 56, pp. 155.

12. R. J. Parker, L. Spiccia, B. Moubaraki, K. S. Murray, D. C. R. Hockless, A. D. Rae and A. C. Willis, *Inorg. Chem.*, 2002, **41**, 2489; M. Clemente-Leon, E. Coronado, J. R. Galan-Mascaros, C. J. Gomez-Garcia, T. Woike and J. M. Clemente-Juan, *Inorg. Chem.*, 2001, **40**, 87; F. Bonadio, M. C. Senna, J. Ensling, A. Sieber, A. Neels, H. Stoeckl iEvans and S. Decurtins, *Inorg. Chem.*, 2005, **44**, 969; S. Gao, B. Q. Ma, H. L. Sun and J. R. Li, *J. Solid State Chem.*, 2003, **171**, 201; L. Jiang, X. L. Feng, T. B. Lu and S. Gao, *Inorg. Chem.*, 2006, **45**, 5018.

13. C. Mathoniere, C. J. Nuttall, S. G. Carling and P. Day, *Inorg. Chem.*, 1996, **35**, 1201; M. J. Rosseinsky, K. Prassides and P. Day, *Inorg. Chem.*, 1991, **30**, 2680; P. R. Surjan, I. Mayer and M. Kertesz, *J. Chem. Phys.*, 1982, **77**, 2454; V. G. Storchak, D. G. Eshchenko, J. H. Brewer, G. D. Morris, S. P. Cottrell and S. F. J. Cox, *Phys. Rev. Lett.*, 2000, **85**, 166; A. J. Marks and K. Prassides, *J. Chem. Phys.*, 1993,

98, 4805; V. P. Coropceanu and K. Prassides, *Chem. Phys. Lett.*, 1998, **289**, 53; C. Achim, E. L. Bominaar, J. Meyer, J. Peterson and E. Munck, *J. Am. Chem. Soc.*, 1999, **121**, 3704; T. Glaser, F. Kesting, T. Beissel, E. Bill, T. Weyhermuller, W. Meyer-Klaucke and K. Wieghardt, *Inorg. Chem.*, 1999, **38**, 722; F. Paul, W. E. Meyer, L. Toupet, H. J. Jiao, J. A. Gladysz and C. Lapinte, *J. Am. Chem. Soc.*, 2000, **122**, 9405.

14. P. Albores, L. D. Slep, L. M. Baraldo, R. Baggio, M. T. Garland and E. Rentschler, *Inorg. Chem.*, 2006, **45**, 2361.

15. N. Y. Zhu and H. Vahrenkamp, *J. Organomet. Chem.* , 1999, **573**, 67.

16. D. E. Richardson and H. Taube, *Coord. Chem. Rev.*, 1984, **60**, 107; W. Kaim, A. Klein and M. Glockle, *Acc. Chem. Res.*, 2000, **33**, 755.

17. Y. Wang, X. Ma, S. M. Hu, Y. H. Wen, Z. Z. Xue, X. Q. Zhu, X. D. Zhang, T. L. Sheng and X. T. Wu, *Dalton Trans.*, 2014, **43**, 17453.

18. Y. Wang, X. Ma, S. M. Hu, Z. Z. Xue, Y. H. Wen, T. L. Sheng and X. T. Wu, *J. Coord. Chem.*, 2015, **68**, 55.

19. C. A. Bignozzi, R. Argazzi, J. R. Schoonover, K. C. Gordon, R. B. Dyer and F. Scandola, *Inorg. Chem.*, 1992, **31**, 5260; B. J. Coe, T. J. Meyer and P. S. White, *Inorg. Chem.*, 1995, **34**, 3600.

20. C. A. Bignozzi, S. Roffia, C. Chiorboli, J. Davila, M. T. Indelli and F. Scandola, *Inorg. Chem.*, 1989, **28**, 4350; V. Comte and H. Vahrenkamp, *J. Organomet. Chem.* , 2001, **627**, 153; D. F. Shriver and J. Posner, *J. Am. Chem. Soc.*, 1966, **88**, 1672.

21. C. A. Bignozzi, R. Argazzi, G. F. Strouse and J. R. Schoonover, *Inorg. Chim. Acta*, 1998, **276**, 380; A. A. Schilt, *Inorg. Chem.*, 1964, **3**, 1323.

22. W. M. Laidlaw and R. G. Denning, *J. Chem. Soc., Dalton Trans.*, 1994, 1987; J. R. Schoonover, C. J. Timpson and T. J. Meyer, *Inorg. Chem.*, 1992, **31**, 3185.

23. E. M. J. Johansson, M. Odelius, S. Plogmaker, M. Gorgoi, S. Svensson, H. Siegbahn and H. Rensmo, *J. Phys. Chem. C*, 2010, **114**, 10314.

24. M. B. Robin and P. Day, *Adv. Inorg. Chem.*, 1968, **10**, 247.

25. S. Margadonna, K. Prassides and A. N. Fitch, *Angew. Chem. Int. Ed.*, 2004, **43**, 6316; D. Papanikolaou, S. Margadonna, W. Kosaka, S. Ohkoshi, M. Brunelli and K. Prassides, *J. Am. Chem. Soc.*, 2006, **128**, 8358; A. Arulraj, A. Biswas, A. K. Raychaudhuri, C. N. R. Rao, P. M. Woodward, T. Vogt, D. E. Cox and A. K. Cheetham, *Phys. Rev. B*, 1998, **57**, R8115; P. M. Woodward, D. E. Cox, E. Moshopoulou, A. W. Sleight and S. Morimoto, *Phys. Rev. B*, 2000, **62**, 844; C. J. Kepert, M. Kurmoo and P. Day, *Inorg. Chem.*, 1997, **36**, 1128; P. Day, N. S. Hush and R. J. H. Clark, *Philos. Trans. R. Soc. A-Math. Phys. Eng. Sci.*, 2008, **366**, 5.

26. O. Kahn, *Molecular Magnetism*, VCH, New York, 1993.

27. W. E. Buschmann, L. Liable-Sands, I. L. Rheingold and J. S. Miller, *Inorg. Chim. Acta*, 1999, **284**, 175.

28. A. A. Schilte, *J. Am. Chem. Soc.*, 1963, **85**, 904; G. Bryant, J. Fergusson and H. Powell, *Aust. J. Chem.*, 1971, **24**, 257.

29. A. A. Schilt, *J. Am. Chem. Soc.*, 1960, **82**, 3000; A. A. Schilt, P. A. Russo and A. Wold, *Inorg. Synth.*, 1970, 247.

30. B. F. Hallam and P. L. Pauson, *J. Chem. Soc.*, 1956, 3030; P. M. Treichel and D. C. Molzahn, *Synth. React. Inorg. Met.-Org. Chem.*, 1979, **9**, 21.

31. G. M. Sheldrick, *SHELXL-97*, (1997) University of Göttingen, Germany

Influence of the central diamagnetic cyanidometal on the distant magnetic interaction in cyanide-bridged Fe(III)-M(II)-Fe(III) complexes

Yong Wang,[a] Chensheng Lin,[a] Xiao Ma,[a] Zhenzhen Xue,[a] Xiaoquan Zhu,[a]   Wenhai Cao,[a] Shengmin Hu,[a] Tianlu Sheng*[a] and Xintao Wu[a]

[a] *State Key Laboratory of Structure Chemistry, Fujian Institute of Research on the Structure of Matter, Chinese Academy of Sciences, Fuzhou, 350002, China. E-mail: tsheng@fjirsm.ac.cn.*

Complexes **1-4** and their oxidation products **5-11** were obtained and investigated. This work shows that for the investigated Fe^{III}-NC-M^{II}-CN-Fe^{III} complexes the magnetic coupling strength between the distant Fe^{III} ions increases with the diamagnetic cyanidometal bridge in the order of Fe < Ru < Os.